ELSEVIER

Catalysis Today 46 (1998) 185–192

CATALYSIS TODAY

Unraveling mechanistic features for the methane reforming by carbon dioxide over different metals and supports by TAP experiments

Y. Schuurman, C. Marquez-Alvarez, V.C.H. Kroll, C. Mirodatos*

Institut de Recherches sur la Catalyse, C.N.R.S. 2, Avenue A. Einstein, F-69626, Villeurbanne Cédex, France

Abstract

Four different catalysts (Ni/SiO_2, Ni/Al_2O_3, Ru/SiO_2, Ru/Al_2O_3) were extensively investigated in the TAP reactor, in order to elucidate the role of the metal and support in the dry reforming of methane. Over nickel, dissociative CH_4 adsorption leads to H_2 gas and to an accumulation of carbon species on the surface. Dissociative CO_2 adsorption takes place giving CO gas and adsorbed oxygen. The latter reacts with carbon, originating from CH_4, on the surface to give a second CO molecule in the rate determining step. Over ruthenium, the methane activation is the slowest step and CO_2 reacts directly with adsorbed carbon to CO. The surface oxygen accumulation is minimal and therefore, the oxidation hydrogen is suppressed. Whereas, the silica support is rather inert, the alumina support participates in the reaction by delivering oxygen atoms to the metal via hydroxyl groups spill-over. In addition, a strong interaction between gaseous CO/CO_2 and oxygenated adspecies is observed on alumina. The reverse water gas shift reaction takes place under the TAP conditions. The different results are discussed in terms of the hydrogen selectivity.

Keywords: Methane reforming; Ruthenium; Nickel; Support; TAP

1. Introduction

The reforming of methane by carbon dioxide into synthesis gas is known to be catalyzed by most of the group VIII metals of which Rh, Ru, Ir and Ni are the most active [1–3]. There is still some debate on the reaction mechanism. A dissociative methane and carbon dioxide adsorption is proposed by Rostrup–Nielsen and Bak-Hansen [1] (different metals) and by Kroll et al., [3] (Ni/SiO_2). The rate determining step is then the recombination of carbon and oxygen on the surface. For the CO_2 reforming over Ir and Ru on alumina, Mark and Maier [2] propose a mechanism where the dissociative methane adsorption is rate limiting, followed by the direct reaction of CO_2 with adsorbed carbon. They observed no effect of the support for Rh and Ir catalysts on the reaction rate. Erdöhelyi et al. [4,5] as well observed no effect of the support (TiO_2, Al_2O_3, MgO, SiO_2) on the turnover frequency for the dry methane reforming over Rh, but they did observe an effect over Pd. The CO/H_2 ratio was between 1.5 and 1.7 for all catalysts (Rh and Pd) except in the case of the Rh/Al_2O_3 catalyst for which a value of 2.6 was found. In contrast, an active role of the support has been proposed in the reaction mechanism over a Ni/La_2O_3 catalyst [6].

In order to further elucidate both the role of the metal and of the support, temporal analysis of products (TAP) experiments were carried out with different catalysts for the methane dry reforming. This fast

*Corresponding author.

0920-5861/98/$ – see front matter
PII: S0920-5861(98)00340-X

transient kinetic method was found to apply perfectly to the mechanistic study of the various reactions dealing with methane activation [7,8]. Preliminary TAP data obtained on Ni- and Ru- silica supported catalysts were presented in [9] and showed a major effect of the metal on the overal kinetics. This paper presents further data and discussion obtained on the following series of dry reforming catalysts: Ni/SiO_2, Ni/Al_2O_3, Ru/SiO_2, Ru/Al_2O_3.

2. Experimental

2.1. Catalysts

The nickel was supported on silica (Degussa Aerosil 200, S_{BET}=180 $m^2\ g^{-1}$) and on α-alumina (Martinswerk, S_{BET}=9 $m^2\ g^{-1}$) by impregnation with a $Ni(NH_3)_6NO_3$ solution and a $NiCO_3$ solution, respectively. After drying, the catalysts were calcined in air at 750°C for 15 h. The metal dispersion was determined by magnetic measurements after reduction of the samples in H_2 at several temperatures, using the Weiss method, which was shown to compare satisfactorily with dispersion measured by H_2 volumetry and electron microscopy [10].

The ruthenium catalysts were prepared by impregnation of the supports (silica, Degussa Aerosil 200, S_{BET}=180 $m^2\ g^{-1}$ and γ-alumina, Puralox Condea, S_{BET}=175 $m^2\ g^{-1}$) with aqueous solutions of ruthenium chloride (Aldrich Chemie). The samples were dried and then calcined at 500°C. After reduction in H_2 at 400°C for 2 h, the dispersion was measured by H_2 pulse chemisorption at 100°C.

The steady-state activity of the catalysts was measured in a recycle reactor with a recycle ratio of at least 20 to attain perfectly mixed conditions. The CH_4/CO_2 ratio of the inlet feed was fixed to 1 (CH_4:CO_2:He= 15:15:70 and 10:10:80 for nickel and ruthenium catalysts, respectively).

Metal loading, dispersion and turnover frequency for all catalysts are given in Table 1.

2.2. TAP experiments

A TAP experiment consists of introducing narrow gas pulses of reactants in a microreactor which is evacuated continuously. The response of this pulse is detected by a quadrupole mass spectrometer at the reactor exit. The shape of the response reflects diffusion, adsorption, desorption and reaction of the reactants and products. The principle of the TAP experiment and its applications are extensively described by Gleaves et al. [11,12].

The commercial TAP-2 reactor contains four high-speed pulse valves, a microreactor, a liquid nitrogen trapped vacuum system, and a quadrupole mass spectrometer located directly underneath the reactor exit. The microreactor measures 25.4 mm in length and 4.1 mm in diameter. A heating element is wrapped around the reactor and is controlled by a temperature controller which reads the output of the thermocouple located in the catalyst bed.

The samples were reduced under a flow of hydrogen at 500°C for the nickel and at 400°C for the ruthenium catalysts. After 1 h the flow was stopped and the reactor evacuated and heated to 550°C for the Ru catalysts and to 600°C for the Ni catalysts. Alternating pulse experiments were performed with a 9/1 $^{12}CH_4$/Ar mixture in one valve and $^{13}CO_2$ in the other valve (10^{14} molecules/pulse). Note that actually around 20 sequences of the two $^{12}CH_4$ and $^{13}CO_2$ pulses were done for each experiment and averaged to give the responses presented in the result section.

Table 1
Catalysts characterization data and catalytic properties

Catalyst	Metal loading (wt%)	Metal dispersion (%)	Reduction temperature (°C)	Degree of reduction (%)	Temperature of reaction (°C)	Turn-over frequency (s^{-1})
Ni/SiO_2	4.0	10	700	97	700	5.0
Ni/α-Al_2O_3	4.3	17	750	62	700	7.2
Ru/SiO_2	0.7	13	400	nd[a]	550	3.5
Ru/γ-Al_2O_3	0.6	51	400	nd[a]	550	1.0

[a]not determined.

3. Results

Table 1 shows that the metal dispersions for the different catalysts are about the same, except for the Ru/Al_2O_3 which is significantly higher. The steady-state turn-over frequencies for all four catalysts are the same order of magnitude, making the Ru the more active metal, since these catalytic tests were performed at lower temperature of 550°C. In the next sections we will describe the specific features for each catalyst as observed during a TAP $^{12}CH_4/^{13}CO_2$ pump-probe experiment. The methane conversion, the hydrogen selectivity and the residence times of the products for these experiments are reported in Table 2.

3.1. Ni/SiO_2

Fig. 1, already presented in [9], shows the transient responses of the reactants and products on a pulse of $^{12}CH_4$/Ar followed 0.5 s later by a pulse of $^{13}CO_2$ over Ni/SiO_2. An evolution of hydrogen gas takes place on the methane pulse. Two distinct carbon monoxide responses are observed on the labeled carbon dioxide pulse: the first corresponding to ^{13}CO formed instantly, the second delayed and tailing, corresponding to ^{12}CO. The time interval between the pulses was varied between 0 and 2 s but it did not influence conversions or selectivity.

The reaction of CH_4 over nickel was studied in more detail by first pretreating the Ni/SiO_2 sample with a series of CO_2 pulses until the conversion dropped to zero. Next a series of methane pulses was started and the methane, hydrogen and carbon monoxide transient responses were monitored as a function of pulse number. Fig. 2 shows the integrated responses versus pulse number. During the first few pulses of methane, the methane conversion is low and a production of CO is observed. The CO production drops off rapidly to a more steady level which then

Table 2
Methane conversion, hydrogen selectivity and residence time of product and inert gases in the TAP experiments

Catalyst	X_{CH4}	S_{H2}	Residence time (s)			
			Ar	H_2	^{13}CO	^{12}CO
Ni/SiO_2	0.87	0.10	0.05	0.06	0.07	0.35
$Ni/\alpha\text{-}Al_2O_3$	0.99	0.01	0.06	0.20		
Ru/SiO_2	0.50	0.95	0.06	0.05	0.10	0.10
$Ru/\gamma\text{-}Al_2O_3$	0.75	0.67	0.05	0.11	0.25	0.23

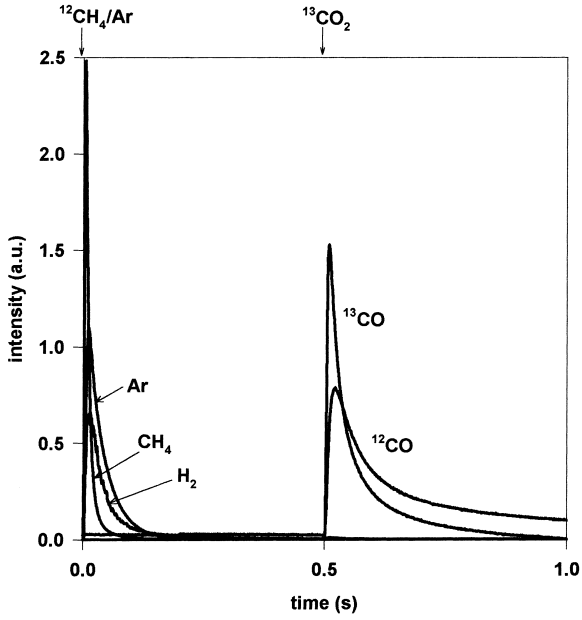

Fig. 1. Double pulse experiment, $^{12}CH_4$/Ar (9/1) followed by $^{13}CO_2$ over a Ni/SiO_2 catalyst (26 mg) at 600°C [9].

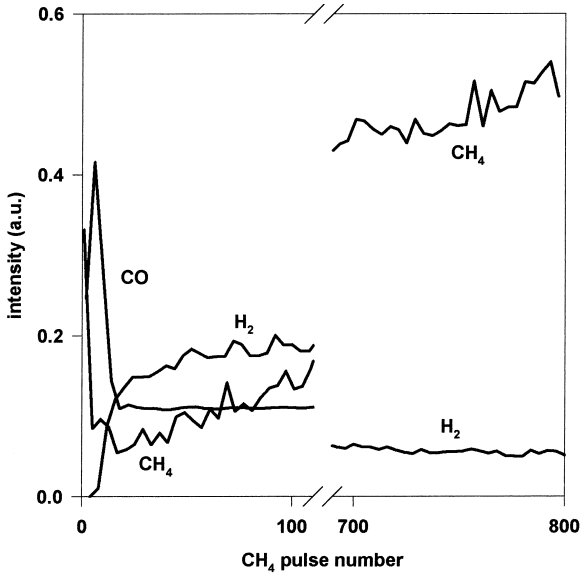

Fig. 2. Multipulse experiment, $^{12}CH_4$/Ar (9/1), after a multipulse pretreatment by $^{13}CO_2$ over a Ni/SiO_2 catalyst (26 mg) at 600°C.

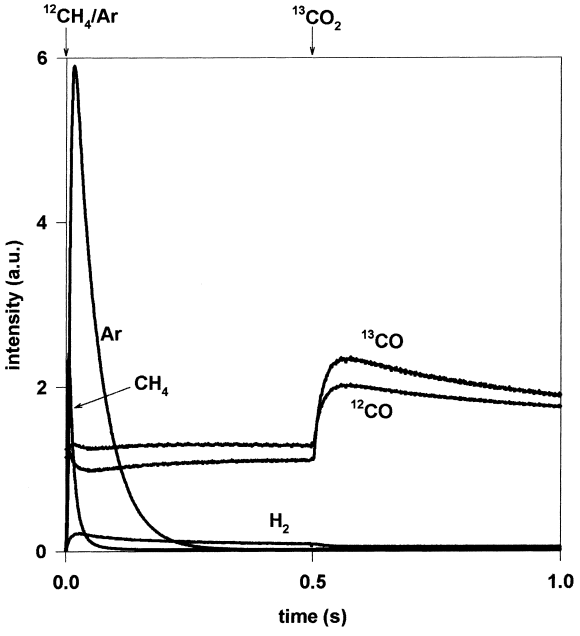

Fig. 3. Double pulse experiment, $^{12}CH_4$/Ar (9/1) followed by $^{13}CO_2$ over a Ni/Al_2O_3 catalyst (30 mg) at 600°C.

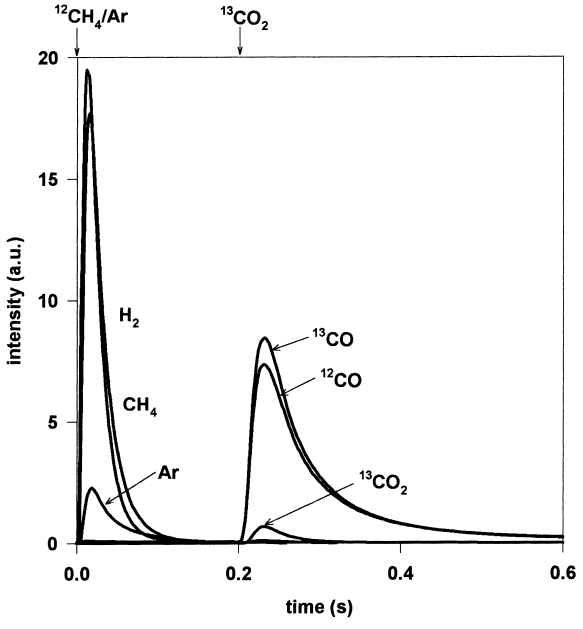

Fig. 4. Double pulse experiment, $^{12}CH_4$/Ar (9/1) followed by $^{13}CO_2$ over a Ru/SiO_2 catalyst (65 mg) at 550°C [9].

slowly decreases with increasing methane pulse number. At the same time the methane conversion goes up and then slowly decreases. No hydrogen is observed on the first few methane pulses, but a maximum in the hydrogen production occurs around 200 methane pulses after which the production slowly decreases.

During this experiment the CO pulse response changes dramatically. At first a fast CO response is observed which is getting more disperse as the methane pulsing continues. It eventually results in a continuous signal which then slowly decreases to zero. The hydrogen response gradually becomes broader and the pulse maximum shifts towards longer times.

3.2. *Ni/α-Al_2O_3*

The same TAP $^{12}CH_4/^{13}CO_2$ experiment carried out over Ni/Al_2O_3, shown in Fig. 3, resulted in broader responses of both hydrogen and carbon monoxide. The CO response has become a continuous signal with a superposition of the transient response. The hydrogen response decreases suddenly on the introduction of the carbon dioxide pulse. Moreover, the hydrogen selectivity is much lower than over Ni/SiO_2 (Table 2).

3.3. *Ru/SiO_2*

In the case of a Ru/SiO2 catalyst, the TAP $^{12}CH_4/^{13}CO_2$ experiment revealed a different behavior than over nickel (Fig. 4) [9]. Again the hydrogen production was observed upon the introduction of methane with a very high selectivity (Table 2). On the $^{13}CO_2$ pulse, the ^{12}CO and ^{13}CO responses were identical.

Fig. 5 shows the integrated responses for a multipulse methane experiment over Ru/SiO_2 equivalent to the one described above for Ni/SiO_2. Here too, a different behavior is observed over Ru than over Ni. At the first pulses, the methane conversion and the hydrogen production are at their maximum, then further decreasing with increasing pulse number. The hydrogen response becomes gradually broader with increasing pulse number. Only on the first methane pulse a broad CO response is found.

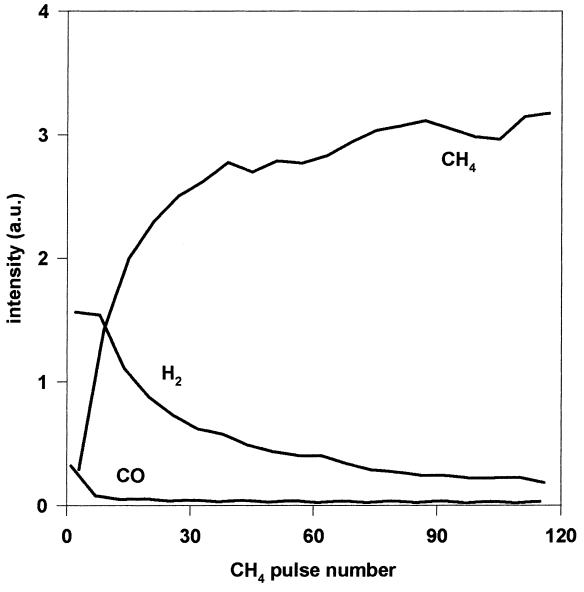

Fig. 5. Multipulse experiment, $^{12}CH_4$/Ar (9/1), after a multipulse pretreatment by $^{13}CO_2$ over a Ru/SiO_2 catalyst (65 mg) at 550°C.

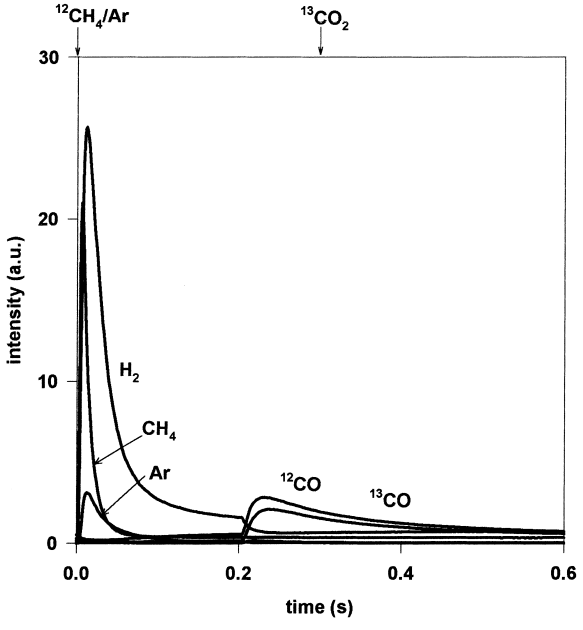

Fig. 6. Double pulse experiment, $^{12}CH_4$/Ar (9/1) followed by $^{13}CO_2$ over a Ru/Al_2O_3 catalyst (67 mg) at 550°C.

3.4. *Ru/γ-Al_2O_3*

The TAP $^{12}CH_4/^{13}CO_2$ experiment is shown in Fig. 6. Hydrogen is produced on the methane pulse and its response tails considerably, until the introduction of $^{13}CO_2$, upon which a sudden consumption of hydrogen appears. The methane conversion is higher with a lower selectivity for hydrogen as compared to the Ru/SiO_2 catalyst. On the methane pulse the ^{12}CO production already starts, with a superposition of the transient production on the $^{13}CO_2$ pulse. The ^{12}CO and ^{13}CO responses corresponding to the $^{13}CO_2$ pulse are identical but significantly broader than those observed over Ru/SiO_2. The $^{13}CO/^{12}CO$ ratio changes significantly with the $^{13}CO_2$ pulse intensity; bigger $^{13}CO_2$ pulses lead to a higher $^{13}CO/^{12}CO$ ratio.

4. Discussion

Significant changes in the TAP responses (shape and intensity) are found according to the nature of the metal and/or of the support, clearly indicating changes in the kinetics of methane reforming depending on the tested catalyst.

4.1. *Role of the metal*

The role of the metal can be outlined by comparing Ni and Ru catalysts supported on silica, which may be considered as an inert support [9]. Over Ni/SiO_2 (Fig. 1), the production of hydrogen takes place on the methane pulse and this step can be written as follows:

$$^{12}CH_4 + Ni \rightleftarrows Ni^{12}C + 2H_2 \quad (1)$$

Actually, the step (1) most probably involves the intermediate formation of hydrogenated species CH_x and a fast and largely reversible gas/surface hydrogen equilibrium. As a matter of fact, fast H/D exchange reactions were observed when switching from CH_4 to CD_4 at the reactor inlet under steady-state conditions, as detailed in [3]. However, the step (1) leads to the accumulation of stable surface carbon monomers able to form up to a monolayer of surface carbide, as demonstrated by temperature programmed hydrogenation experiments and XPS evidences [3]. It can be noted however in Table 2 that a large part of the hydrogen produced from the methane cracking suffers a further oxidation under the TAP conditions.

From the observation of two completely distinct responses for unlabeled and labeled CO, two different routes for the production of CO were considered over Ni/SiO_2, represented by:

$$^{13}CO_2 + Ni \rightleftarrows Ni - O_{ads} + {}^{13}CO \quad (2)$$

$$Ni - O_{ads} + Ni^{12}C \rightarrow 2Ni + {}^{12}CO \quad (3)$$

In step (2), the dissociative adsorption of CO_2 leads to surface oxygen and gaseous CO, since no oxygen release is observed. In contrast, CO is immediately released into the gas phase, as indicated by the absence of tailing for the corresponding TAP response. This step (2), strongly displaced towards the dissociation under TAP conditions (almost complete CO_2 conversion) was shown to be equilibrated under steady-state conditions by observing similar isotopic composition between CO and CO_2 [3].

Step (3) corresponds to the reaction of surface carbon monomers (arising from step (1)) with surface oxygen atoms (arising from step (2)) into CO slowly released into the gas phase, as revealed by the important tailing of the related TAP response. This slow step 3 was proposed as rate limiting for the reforming process over Ni/SiO_2 catalyst [3,9]. As a matter of fact, no isotopic effect was observed for the overall methane and carbon dioxide conversion, indicating that the RDS of the process does not involve C-H bond cleavage or formation [3].

Another indication that the surface oxygen produced upon CO_2 activation (step 2) is stable enough to react with surface carbon is that the hydrogen formed from methane cracking in step (1) is readily oxidized though no more gaseous CO_2 crosses the catalytic bed. Thus, the following step must be added to the mechanism:

$$H_2 + Ni - O_{ads} \rightleftarrows H_2O + Ni \quad (4)$$

Like the step (2), the step (4), strongly displaced towards water formation under tap conditions, is shown to be at equilibrium under steady-state conditions. Thus, the combination of steps (2)+(4) forms the WGS equilibrium, generally achieved under reforming conditions [13].

The presence of oxygen atoms on the nickel surface is also confirmed by the experiment shown in Fig. 2, where after a pretreatment of the nickel catalyst by a series of CO_2 pulses CO formation is observed on a subsequent methane pulses: The CO is formed by the reaction of oxygen atoms accumulated during the series of carbon dioxide pulses and surface carbon formed on the methane pulse (step (3)). Apparently, the methane activation is less effective over a highly oxidized nickel surface, because the conversion of methane is at first low and then starts to increase after the CO production has dropped significantly, corresponding to the decrease in surface oxygen concentration. Indeed the methane conversion decreases again when no more oxygen is available and the surface is saturated with carbon. The CO response broadens quickly with increasing the pulse number indicating a decrease of the formation rate. Thus, the rate of CO formation becomes more and more determined by the diffusion rate of oxygen through the bulk. Similarly, at first hydrogen is completely oxidized to water by the oxygen present on the nickel. With increasing the pulse number the selectivity increases to approximately 70% at the end of the experiment. At the same time the hydrogen response becomes broader, indicating that the rate of methane adsorption (step(1)) slows down when the surface becomes more carbided. Together with a geometric effect of surface poisoning by carbon deposits, an electronic effect could be assumed, since it is well known from single crystal studies that the hydrogen-metal and carbon-metal bonds are weakened on carbided nickel due to the displacement of valency electrons of nickel to the strong Ni-C bonds of the carbide [14,15]. Similar H_2 response braodening was observed by Buyevskaya et al. [16] over Rh and Ru/Al_2O_3 which may also be assigned to carbon deposition on metal.

This mechanism of the dry reforming over Ni/SiO_2 is similar to the one proposed by Rostrup–Nielsen and Bak-Hansen on the basis of the steam-reforming [1].

Over Ru/SiO_2 (Fig. 4), the same step (1) of methane cracking is observed, but leading to a much larger hydrogen production (Table 2).

$$^{12}CH_4 + Ru \rightarrow Ru^{12}C + 2H_2 \quad (5)$$

The latter suggests a much lower concentration of surface oxygen. At variance with Ni/SiO_2, the two CO responses are identical, indicating that they are formed in the same step:

$$^{13}CO_2 + Ru^{12}C \rightleftarrows {}^{13}CO + {}^{12}CO + Ru \quad (6)$$

This implies that no oxygen atoms are present on the ruthenium surface during reaction, which rules out a step equivalent to step (4) for ruthenium, in agreement with the high H_2 selectivity above mentioned. This statement is also confirmed by the experiment shown in Fig. 5, where after a pretreatment of the ruthenium catalyst by a series of CO_2 pulses no significant CO formation is observed on a subsequential methane pulse. Methane activation takes place over the clean ruthenium surface, since hydrogen production is observed.

The reaction step (6) is also proposed by Mark and Maier [2] to explain their data obtained over Ru and Ir/Al_2O_3 catalysts. According to them the methane activation, step (5), is for this case rate determining and the step (6) is fast. This statement that the methane activation becomes slower on ruthenium agrees well with the fact that Ru is known to maintain carbonaceous residue for a longer period than Ni, which favors the chain growth for Fischer–Tropsch synthesis [17].

Hence, the presence of surface oxygen on Ni and its absence on Ru explains the difference in hydrogen selectivity's for the two metals, as reported in Table 2.

4.2. Role of the support

Much broader responses of both CO and H_2 products are observed on the alumina supported catalysts as compared to the silica supported ones (Fig. 3 and Fig. 6), which clearly indicates a major role of the alumina within the catalytic process. This leads for both catalysts to comparable ^{13}CO and ^{12}CO responses, with an almost continuous production along the sequential $^{12}CH_4/^{13}CO_2$ pulse experiments. Similarly, a large tailing of hydrogen is observed on both catalysts, even if the H_2 production remains far more larger on ruthenium than on nickel, as discussed earlier. An important effect to be stressed is also the marked decrease of this continuous H_2 production upon the CO_2 pulse.

γ-alumina is well known to act as a reservoir of hydroxyl groups due to its large concentration of acid and basic sites, which indeed favors the reverse spill-over of OH groups (or adsorbed water) to the metal surface, as clearly demonstrated on partially reduced Ni/Al_2O_3 catalysts by Dalmon et al. in [18]. In turn, these metal hydroxyls will react fast with the carbided metal into H_2 and CO as follows:

$$OH_{Al_2O_3} + Me \rightarrow MeOH \quad (7)$$

$$MeOH + MeC \rightarrow CO + \frac{1}{2}H_2 + Me \quad (8)$$

The consumed alumina hydroxyl groups are regenerated by the water formed during the process (most likely through the reverse WGS reaction as discussed later). A close process of spill-over between alumina and metal but via the migration of water molecules was recently proposed by Wang et al. for the partial oxidation of methane over Rh/Al_2O_3 [19].

Steps (7-8) will thus provide a residual flow of hydrogen and CO longtime after the methane and carbon dioxide pulses, as experimentally observed. In the case of Ru/Al_2O_3 (Fig. 6) it explains the production of ^{12}CO on the methane pulse and the large tailing of the ^{12}CO response. However, the continuous production of CO (labeled and unlabeled) is found much larger than the one of hydrogen over Ni/Al_2O_3 (Fig. 3). This means that for this case, the alumina also acts as a reservoir of reversible CO_2 and/or CO. The following equilibria are probably established with the acid/base groups on the alumina, as suggested by in situ infrared evidence of formate and/or carbonate groups observed specifically on the alumina supported catalysts [unpublished results]:

$$O^{2-} + CO_2 \rightleftarrows CO_3^{2-} \quad (9)$$

$$-OH + {}^{12,13}CO \rightleftarrows -OCHO \quad (10)$$

The latter type of equilibrium was also reported by Amenomiya [20,21].

The difference of alumina chemistry between Ru and Ni could arise from the redox state of the metal particles: a rather high oxygen coverage for the case of Ni would limit the spill-over steps (7–9) and therefore favor the step (11), while the reverse trend would be favored on Ru, maintained under a more reduced state along the experiments. Moreover, α-alumina is far more dehydrated than γ-alumina.

In both cases, the sudden drop of the hydrogen response on the carbon dioxide pulse in Fig. 3 and Fig. 6 confirms the reaction of hydrogen with CO_2 through the overall reverse WGS, favored on alumina via the above spill-over steps (7–8) and CO/formate equilibrium (step 10), as:

$$H_2 + {}^{13}CO_2 \rightleftarrows H_2O + {}^{13}CO \quad (11)$$

This was confirmed by increasing the $^{13}CO_2$ pulse intensity which resulted in an increased ^{13}CO production, while the ^{12}CO response did hardly change.

5. Conclusions

The above TAP study for the four different catalysts gives a direct evidence for common and/or specific features of the CO_2 reforming mechanism. It permits a discrimination of the main elementary steps of methane and carbon dioxide activation and to get direct information about the origin of the formed carbon monoxide. The quantitative evaluation of the hydrogen selectivity can be straight-forwardly related to the secondary oxidation of hydrogen into water. Unlike the silica support, the alumina support plays a intricate role in the mechanism, due to participation of its acid/base groups. The properties of these groups are strongly changed by water, which is a side-product of this reaction. Further modeling of the curves is in progress to provide quantitative kinetic parameters for the main identified elementary steps.

Acknowledgements

The authors thank the Region Rhône-Alpes for their financial support and the Spanish Ministerio de Educacion y Cultura for a post-doctoral grant. Prof. A. Guerrero-Ruiz and I. Rodriguez-Ramos are fully acknowledged for fruitful discussion and for providing Ru samples.

References

[1] J.R. Rostrup-Nielsen, J.H. Bak-Hansen, J. Catal. 144 (1993) 38.
[2] M.F. Mark, W.F. Maier, J. Catal. 164 (1996) 122.
[3] V.C.H. Kroll, H.M. Swaan, S. Lacombe, C. Mirodatos, J. Catal. 164 (1997) 387.
[4] A. Erdöhelyi, J. Cserenyi, F. Solymosi, J. Catal. 141 (1993) 287.
[5] A. Erdöhelyi, J. Cserenyi, E. Papp, F. Solymosi, Appl. Catal. 108 (1994) 205.
[6] A. Slagtern, Y. Schuurman, C. Leclercq, X. Verykios, C. Mirodatos, J. Catal. 172 (1997) 118.
[7] A.N.J. van Keulen, K. Seshan, J.H.B. Hoenink, J.R.H. Ross, JU. Catal. 166 (1997) 306.
[8] Y. Schuurman, C. Mirodatos, Appl. Catal. 151(1) (1997) 305.
[9] Y. Schuurman, V.C.H. Kroll, P. Ferreira-Aparicio, C. Mirodatos, Catal.Today 38 (1997) 129.
[10] M. Primet, J.A. Dalmon, G.A. Martin, J. Catal. 46 (1977) 25.
[11] J.T. Gleaves, J.R. Ebner, T.C. Kuechler, Catal. Rev.-Sci. Eng. 30 (1988) 49.
[12] J.T. Gleaves, G.S. Yablonskii, P. Phanawadee, Y. Schuurman, Appl. Catal. General 160 (1997) 55.
[13] H.M. Swaan, V.C.H. Kroll, G.A. Martin, C. Mirodatos, Proc. 4th European Workshop on Methane Conversion, Eindhoven, 1994, Catal. Today 21 (1994) 571.
[14] J.G. McCarty, R.J. Madix, Surf. Sci 54 (1976) 121.
[15] J.C. Bertolini, B. Tardy, Surf. Sci. 102 (1981) 131.
[16] O.V. Buyevskaya, D. Wolf, M. Baerns, Catal. Lett. 29 (1994) 249.
[17] M. de Pontes, G.H. Yokomiso, A.T. Bell, J. Catal. 104 (1987) 147.
[18] J.A. Dalmon, C. Mirodatos, P. Turlier, G.A. Martin, In: G.M. Pajonk et al. (Eds.), Spillover of Adsorbed Species, Elsevier, Amsterdam, 1983, p. 169.
[19] D. Wang, O. Dewaele, A.M. De Groote, G. Froment, J. Catal. 159 (1996) 418.
[20] Y. Amenomiya, J. Catal. 55 (1978) 205.
[21] Y. Amenomiya, G. Pleizer, J. Catal. 76 (1982) 345.